Journal of Mathematical Biology manuscript No.
(will be inserted by the editor)

Y Timofeeva · S Coombes

Wave bifurcation and propagation failure in a model of Ca^{2+} release

the date of receipt and acceptance should be inserted later –

Abstract. The De Young Keizer model for intracellular calcium oscillations is based around a detailed description of the dynamics for inositol trisphosphate (IP_3) receptors. Systematic reductions of the kinetic schemes for IP_3 dynamics have proved especially fruitful in understanding the transition from excitable to oscillatory behaviour. With the inclusion of diffusive transport of calcium ions the model also supports wave propagation. The analysis of waves, even in reduced models, is typically only possible with the use of numerical bifurcation techniques. In this paper we review the travelling wave properties of the biophysical De Young Keizer model and show that much of its behaviour can be reproduced by a much simpler Fire-Diffuse-Fire (FDF) type model. The FDF model includes both a refractory process and an IP_3 dependent threshold. Parameters of the FDF model are constrained using a comprehensive numerical bifurcation analysis of solitary pulses and periodic waves in the De Young Keizer model. The linear stability of numerically constructed solution branches is calculated using pseudospectral techniques. The combination of numerical bifurcation and stability analysis also allows us to highlight the mechanisms that give rise to propagation failure. Moreover, a kinematic theory of wave propagation, based around numerically computed dispersion curves is used to predict waves which connect periodic orbits. Direct numerical simulations of the De Young Keizer model confirm this prediction. Corresponding travelling wave solutions of the FDF model are obtained analytically and are shown to be in good qualitative agreement with those of the De Young Keizer model. Moreover, the FDF model may be naturally extended to include the discrete nature of calcium stores within a cell, without the loss of analytical tractability. By considering calcium stores as idealised point sources we are able to explicitly construct solutions of the FDF model that correspond to saltatory periodic travelling waves.

1. Introduction

Ca^{2+} is critically important for a large number of cellular functions, such as muscle contraction, cardiac electrophysiology, bursting oscillations, synaptic plasticity, sensory perception and adaptation in photoreceptors (Berridge

Department of Mathematical Sciences, Loughborough University, Loughborough, Leicestershire, LE11 3TU, UK

Correspondence to: S Coombes e-mail: `s.coombes@lboro.ac.uk`

Key words: Calcium waves – stability – lattice models

[1997]). It is stored intracellularly in the endoplasmic reticulum (ER) or sarcoplasmic reticulum (SR) at 2-3 orders of magnitude greater than its concentration in the cytosol. Ca^{2+} signalling in a wide diversity of cell types frequently occurs as repetitive, but transient, increases in Ca^{2+} concentration. Changes in cytosolic $[Ca^{2+}]$ are controlled, in part, by Ca^{2+} channels in the surface membrane and the release of Ca^{2+} from internal stores In this latter case, distinctions can be made on the basis of whether the release of Ca^{2+} is dominated by the ryanodine receptor, the inositol (1,4,5)-trisphosphate (IP_3) receptor, a combination of both of these or an unregulated leak (Sneyd et al. [1995]). The IP_3 receptors are Ca^{2+} channels which are opened by the binding of IP_3, generating a gradient-driven flux of Ca^{2+} from the ER into the cytosol. Ryanodine receptors are Ca^{2+} sensitive and control the release of Ca^{2+} from the SR. The major source of Ca^{2+} release from internal stores in cardiac and skeletal muscle is from ryanodine receptors, whilst IP_3 receptors are the major source of release from internal stores in non-muscle cells. The amount of Ca^{2+} released, in response to a triggering event, can be considerably greater than the initial flux of Ca^{2+}, but only if this initial flux exceeds some threshold (Callamaras et al. [1998]). In the case of IP_3 receptors, the autocatalytic release of Ca^{2+} terminates once $[Ca^{2+}]$ reaches a sufficiently high level. Beyond this level processes which take up Ca^{2+} from the cytosol dominate the dynamics. These involve transport of Ca^{2+} into the extracellular medium and into the SR by exchangers and pumps located in the cell membranes. This is an example of a nonlinear feedback process, often referred to as Ca^{2+}-induced Ca^{2+} release (CICR), and is thought to be one of the mechanisms underlying wave propagation (Allbritton and Meyer [1993]). Travelling waves of Ca^{2+} concentration are believed to be an important means for coordinating cellular activity over large regions (Callamaras et al. [1998]). These waves involve diffusion of locally released Ca^{2+} to neighbouring release sites, causing neighbouring channels to open and release more Ca^{2+}, which in turn diffuses. Waves can be initiated from sites of oscillatory Ca^{2+} release or by a transient local release of Ca^{2+} termed a Ca^{2+} spark (Lipp and Bootman [1997]).

The work in this paper is broadly concerned with the propagation and propagation failure of Ca^{2+} waves in IP_3 sensitive systems. We begin with a study of one of the more popular models underlying Ca^{2+} waves and oscillations, namely the De Young Keizer model (De Young and Keizer [1992]). Our first aim is to use a systematic numerical bifurcation analysis to obtain as much information as possible about travelling wave solutions in this model. Our second and major goal is to construct a Fire-Diffuse-Fire (FDF) type model that can capture the essential behaviour of the more complicated biophysical model. The FDF model (Keizer et al. [1998]) models spark mediated wave propagation in terms of a simple threshold process. Although useful in describing the propagation of solitary waves it is unsuitable for general application since it lacks any notion of a recovery variable. Moreover, although originally intended to model a system based on ryanodine receptors (namely the heart) we show how it may be generalised

to cover the case of IP_3 receptors. To summarise, we present a generalised FDF type model, constrained by the biologically plausible De Young Keizer model, that includes both a refractory process and IP_3 sensitivity. This is important since it opens the way for a comprehensive mathematical analysis of realistic Ca^{2+} waves.

In section 2 we introduce the De Young Keizer model and its reduction to a so-called two-state model using the techniques of Li and Rinzel (1994). Travelling waves are identified as stationary solutions in an appropriate comoving reference frame. The linear stability of wave solutions is treated as an eigenvalue problem.

In section 3 we present our numerical analysis of the De Young Keizer model. Periodic waves are viewed as periodic solutions to a set of travelling wave ODEs and solitary pulses as homoclinic orbits. In either case standard numerical techniques are used to construct and continue solutions in parameter space. The eigenvalue problem that must be solved in order to determine linear stability of solutions is performed numerically using pseudospectral techniques. The solitary pulse is shown to have a bifurcation structure entirely consistent with that of the two-state IP_3 receptor model of Sneyd et al. (2000), including an interesting set of global bifurcations. In this section we also present a kinematic theory of wave propagation based around numerically computed dispersion curves for periodic waves. We use this to predict the existence of a non-periodic wave that may be regarded as a travelling front that connects two different periodic orbits. Direct numerical simulation of the De Young Keizer model confirms this prediction.

In section 4 we identify the essential features of the De Young Keizer model that must be present in a simpler model for it to produce qualitatively the same behaviour as that found in section 3. We present a generalised FDF model with an IP_3 dependent threshold and a simple refractory process with parameters constrained using numerical data from the De Young Keizer model. A mathematical analysis of periodic travelling waves is used to highlight the ability of the generalised FDF model to describe realistic travelling Ca^{2+} waves. We then consider the case that calcium stores are located at discrete sites in a cell. This simple change to any continuum model of calcium waves has highly non-trivial consequences since it destroys translation invariance (and invalidates many of the standard tools of analysis). However, within the FDF framework analytical progress is still possible. To illustrate this point we explore the consequences of discreteness on propagation failure for saltatory periodic travelling waves.

Finally in section 5 we summarise the major points of this paper and discuss natural extensions of our work.

2. The De Young Keizer model

De Young and Keizer (1992) developed a detailed molecular model of a subunit of the IP_3 receptor that included the binding of one activating IP_3 and two Ca^{2+} ions, the second of which produced an inhibited state of the

subunit (see the book by Keener and Sneyd 1998 for an excellent review). These subunits are treated as independent and identical; only when three of the subunits have both IP_3 and an activating Ca^{2+} bound is the IP_3 receptor regarded as in the open state. In more detail there are three sites on each subunit; an IP_3 binding site, an activating Ca^{2+} binding site and an inactivating Ca^{2+} site. Each state of the subunit is given by x_{ijk}, $i, j, k \in \{0, 1\}$, where the first index refers to the IP_3 binding site, the second to the Ca^{2+} activation site, and the third to the Ca^{2+} inactivation site. If any of the indices i, j or k are equal to 1, then a binding site is occupied. Otherwise the binding site is unoccupied. The eight possible receptor states are presented in figure 1, where p and c denote IP_3 and Ca^{2+} concentrations respectively. The coefficients k_i, k_{-i}, $i = 1, \ldots, 5$ parameterise the transitions between the different receptor states.

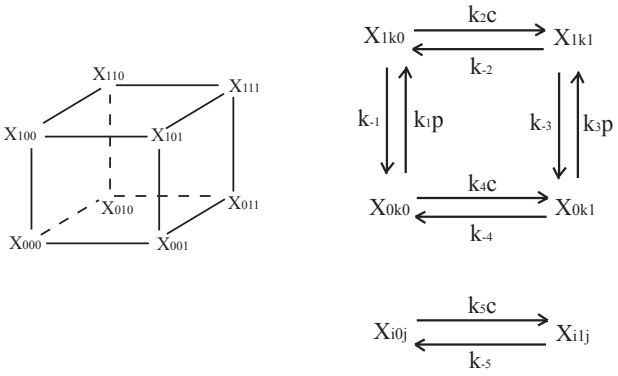

Fig. 1. Schematic binding diagram for the IP_3 receptor model of De Young and Keizer.

Seven differential equations based on mass-action kinetics together with the constraint $\sum_{i,j,k} x_{ijk} = 1$ (conservation of probability) form a mathematical model of the IP_3 receptor. The model assumes that the IP_3 receptor releases Ca^{2+} only when three subunits are in the state x_{110} i.e. with one IP_3 and one activating Ca^{2+} bound. Thus the open probability of the receptor is x_{110}^3. The De Young Keizer model is completed with the following differential equation for Ca^{2+} dynamics:

$$\frac{\mathrm{d}c}{\mathrm{d}t} = (r_1 x_{110}^3 + r_2)(c_{\mathrm{er}} - c) - \frac{r_3 c^2}{c^2 + k_p^2}, \tag{1}$$

where c_{er} denotes the concentration of Ca^{2+} in the ER. The first term in this equation is the Ca^{2+} flux through the IP_3 receptor, and it is proportional to the concentration difference between the ER and the cytosol. The constant r_2 characterises an IP_3-independent leak from the ER into the cytosol. The second term in (1) describes the action of Ca^{2+} ATPases that

pump Ca^{2+} from the cytosol into the ER. Experimental data shows that the Ca^{2+} ATPase is cooperative, with a Hill coefficient of 2.

In a series of papers (Keizer and Young [1994], Li and Rinzel [1994], Tang et al. [1996]) it has been suggested that the experimental observation that IP_3 and Ca^{2+} bind quickly to the activating site can be used to obtain a reduced receptor model. By regarding the receptor as being in a quasi-steady state with respect to IP_3 binding and Ca^{2+} activation the eight differential equations describing the full De Young Keizer model may be reduced to just two. In the reduced model the variable $h = x_{000} + x_{010} + x_{100} + x_{110}$ (a linear combination of so-called group I states) plays a fundamental role. The reduced model is given by (1) with

$$x_{110} = \frac{pch}{(p + K_1)(c + K_5)}, \qquad K_i = k_{-i}/k_i,\ i = 1, \ldots, 5. \tag{2}$$

The dynamics of the inactivation variable h is reminiscent of that of the gating variables in the Hodgkin-Huxley model of nerve membrane and is written in the form

$$\tau(c)\frac{\mathrm{d}h}{\mathrm{d}t} = h_\infty(c) - h, \tag{3}$$

where

$$h_\infty(c) = \frac{\beta}{\alpha(c) + \beta}, \qquad \tau(c) = \frac{1}{\alpha(c) + \beta}, \tag{4}$$

with

$$\alpha(c) = \frac{(k_{-4}K_1K_2 + k_{-2}K_4p)c}{K_2K_4(p + K_1)}, \qquad \beta = \frac{k_{-2}p + k_{-4}K_3}{p + K_3}. \tag{5}$$

A common assumption in many models of intracellular Ca^{2+} waves is that there is also diffusive transport of Ca^{2+} between release sites. Hence, it is natural to add a term $D\nabla^2 c$ to the right hand side of (1). For clarity we shall restrict our attention to one spatial dimension. Since we shall shortly focus on travelling waves with fixed velocity s it is convenient to rewrite the De Young Keizer model in the comoving reference frame where $\xi = x - st$. A transformation into this frame yields

$$\partial_t c = D\partial_\xi^2 c + s\partial_\xi c + f_1(c, h) \tag{6}$$

$$\partial_t h = s\partial_\xi h + f_2(c, h), \tag{7}$$

where

$$f_1(c, h) = (r_1 x_{110}^3 + r_2)(c_{\mathrm{er}} - c) - \frac{r_3 c^2}{c^2 + k_p^2}, \tag{8}$$

$$f_2(c, h) = \frac{h_\infty(c) - h}{\tau(c)}. \tag{9}$$

In the comoving frame, travelling waves with speed s correspond to stationary solutions defined by $\partial_t c = \partial_t h = 0$. Hence, they can be found by studying solutions to the travelling wave ODEs

$$\frac{\mathrm{d}c}{\mathrm{d}\xi} = w, \qquad D\frac{\mathrm{d}w}{\mathrm{d}\xi} = -sw - f_1(c, h), \qquad s\frac{\mathrm{d}h}{\mathrm{d}\xi} = -f_2(c, h). \tag{10}$$

Travelling pulses correspond to a homoclinic orbit in these equations, whilst periodic wave-trains correspond to limit cycle oscillations. Fixed points of the travelling wave ODEs correspond to homogeneous states of the spatially extended model.

Linearisation of (6) and (7) around a stationary (travelling wave) solution $c_0(\xi), h_0(\xi)$ and considering small perturbations of type $(r_j(\xi,t), s_j(\xi,t)) \propto (r_j(\xi), s_j(\xi))\exp(\lambda_j t)$ yields an eigenvalue problem given by

$$\mathcal{M}\begin{bmatrix} r_j(\xi) \\ s_j(\xi) \end{bmatrix} = \lambda_j \begin{bmatrix} r_j(\xi) \\ s_j(\xi) \end{bmatrix}, \qquad \mathcal{M} = \begin{bmatrix} D\partial_\xi^2 + s\partial_\xi + A_1(\xi) & A_2(\xi) \\ B_1(\xi) & s\partial_\xi + B_2(\xi) \end{bmatrix}, \tag{11}$$

where

$$A_1(\xi) = \partial_c f_1(c_0(\xi), h_0(\xi)), \qquad A_2(\xi) = \partial_h f_1(c_0(\xi), h_0(\xi)),$$
$$B_1(\xi) = \partial_c f_2(c_0(\xi), h_0(\xi)), \qquad B_2(\xi) = \partial_h f_2(c_0(\xi), h_0(\xi)).$$

The linear stability of a travelling wave is then determined by an examination of the spectrum of the Jacobian $\mathcal{M}$ in (11). The eigenvalues associated with perturbations around the homogeneous steady state (giving the essential spectrum) can easily be found by substituting solutions of the form $u(\xi,t) = \exp(\lambda t + \mathrm{i}k\xi)u_0$ into the linear equation $u_t = \mathcal{M}u$. Hence, the continuous spectrum of $\mathcal{M}$ is defined by a characteristic polynomial of the form $\det[M(k) - \lambda I] = 0$, where

$$\mathcal{M}(k) = \begin{bmatrix} -Dk^2 + \mathrm{i}sk + A_1 & A_2 \\ B_1 & \mathrm{i}sk + B_2 \end{bmatrix}, \tag{12}$$

where A_1, A_2, B_1 and B_2 are the forms taken by $A_1(\xi)$, $A_2(\xi)$, $B_1(\xi)$ and $B_2(\xi)$ when $(c_0(\xi), h_0(\xi)) = (\bar{c}, \bar{h})$ is a homogeneous steady state. To find the full spectrum of the linearised system it remains to determine the point spectrum of $\mathcal{M}$ (which we shall do numerically). In particular the eigenvalue spectrum of a single pulse in an infinite system contains a continuous part which can be identified with the spectrum of the stable rest state, as well as a discrete part related to eigenfunctions localised near the pulse solution.

3. Travelling waves in the De Young Keizer model

Here we present a numerical analysis of the travelling wave ODEs for the De Young Keizer model given by (10), treating $p = [\mathrm{IP}_3]$ as the physiologically significant bifurcation parameter. All bifurcation diagrams are computed using AUTO as implemented in *xppaut* by Bard Ermentrout (http://www.pitt.edu/∼phase/). Parameter values for the De Young Keizer model are listed in table 1.

We see from figure 2 that the curve of steady states of (10) is folded, so that for a small window of p values there are three solutions. For high and low p there is only stable fixed point. For the parameter values of p where the system has an unstable steady state periodic oscillations occur.

k_1	400 $\mu M^{-1}s^{-1}$	k_{-1}	52 s^{-1}	r_1	20 s^{-1}
k_2	0.2 $\mu M^{-1}s^{-1}$	k_{-2}	0.21 s^{-1}	r_2	0.004 s^{-1}
k_3	400 $\mu M^{-1}s^{-1}$	k_{-3}	377.36 s^{-1}	r_3	1.2 $\mu M^{-1}s^{-1}$
k_4	0.2 $\mu M^{-1}s^{-1}$	k_{-4}	0.029 s^{-1}	k_p	0.1 μM
k_5	20 $\mu M^{-1}s^{-1}$	k_{-5}	1.65 s^{-1}	c_{er}	1 μM

Table 1. Parameters of the De Young Keizer model.

In fact there are two disconnected branches of stable periodic orbits, both of which arise in a homoclinic bifurcation and end in a supercritical Hopf bifurcation. Oscillations of Ca^{2+} first occur with a large period and a very spiky profile. As p increases the period of oscillations rapidly decreases. All

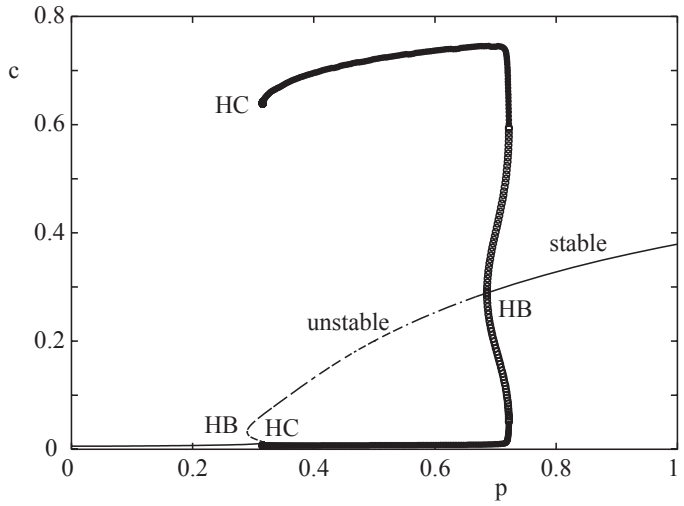

Fig. 2. Bifurcation diagram of the reduced De Young Keizer model when $s = 2$ and $D = 1$. Circles denote amplitude of periodic orbit. HB: Hopf bifurcation; HC: homoclinic bifurcation.

numerically computed homoclinic orbits are just periodic orbits with large period, which for practical purposes we take as 10^4.

In figure 3 we trace the locus of Hopf bifurcations (HB) from figure 2 in the (p, s) plane, as well as three branches of homoclinic orbits (HC) defining travelling pulses. The locus of Hopf bifurcations forms a distinct loop, with only one of the three homoclinic branches (labelled (A)) occupying a significant window of p values. From figure 3 we see that solitary waves on branch A fail to propagate if p is too small. Precisely this form of bifurcation structure has been observed by Sneyd et al. (2000) in a numerical analysis of travelling waves in a model of pancreatic acinar cells. They have discussed this bifurcation diagram in some detail, although without an explicit

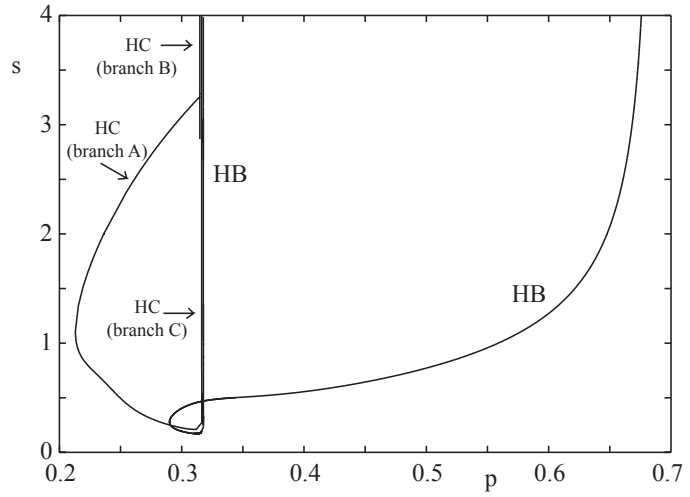

Fig. 3. Two-parameter bifurcation diagram of the travelling wave equations. HB: the curve of Hopf bifurcation points; HC: branches of homoclinic orbits.

determination of wave stability. Using the theory of linear wave stability presented in section 2, we may further develop their arguments. Since, in general, solutions $c_0(\xi)$, $h_0(\xi)$ and the eigenfunctions of the Jacobian $\mathcal{M}$ are not available in closed form, the eigenspectrum of $\mathcal{M}$ has to be determined numerically. We have used Fourier spectral methods (see (Trefethen [2000]) for further discussion) on a bounded domain (with a discretization of 300 points) to do precisely this. The zero eigenvalue, which always exists due to the translational symmetry of the problem, is used as a numerical accuracy check and has been obtained with a precision of 10^{-4}. Figure 4 shows the eigenspectrum for travelling pulse solutions on the upper and lower part of homoclinic branch A in figure 3. We see that, in both cases, the continuous spectrum lies completely in the left complex half-plane. The discrete spectrum for the solution on the upper branch remains in the left half-plane. However, the discrete spectrum for the solution on the lower branch crosses the imaginary axis and has an isolated eigenvalue in the right half-plane. Hence, we conclude that of the two possible coexisting solitary pulses it is the faster one that is stable. We now discuss some further aspects of the bifurcation diagram, figure 3, which are interesting from a dynamical systems perspective.

First of all, we take a closer look at the upper part of homoclinic orbit branch A and show a magnified view of figure 3 in figure 5. The homoclinic branch A is found to end at a T-point. This is a point where a heteroclinic cycle exists between a saddle and a saddle focus. Note that global bifurcations in this model can be directly linked to windows of parameter space where there are three fixed points. Previous work by Glendinning and Spar-

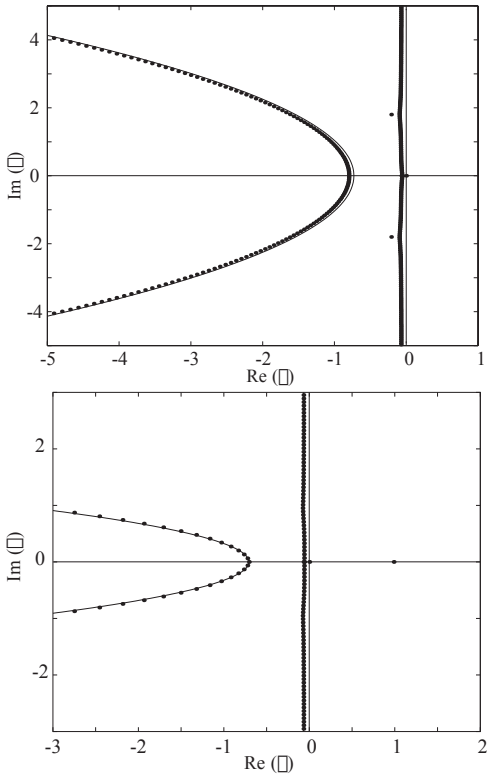

Fig. 4. Left: eigenvalues of the linearised system in the complex plane for the pulse solution at $p = 0.2363$ and $s = 2$. Right: eigenspectrum at $p = 0.2408$ and $s = 0.6$. The solid lines correspond to the analytically obtained continuous spectrum at the same parameter values.

row (1986) predicts the existence of a winding homoclinic branch near a T-point. This phenomenon is clearly seen in figure 5, where the homoclinic branch B connects to homoclinic branch A in a spiral. Next we examine the lower part of homoclinic orbit branch C using the magnified view presented in figure 6. As the speed of travelling wave decreases, folds in the homoclinic branch C occur before the branch intersects a curve of Hopf bifurcation points. Balmforth et al. (1994), have shown that the resulting oscillations in the branch of homoclinic orbits correspond to homoclinic orbits that make multiple loops around one of the other steady states before returning to the starting point. Just such an orbit is presented in figure 7, which is taken from branch C at a point near where the branch intersects the locus of Hopf points.

Using direct numerical simulations Sneyd et al. (2000) also show that secondary waves and irregular behaviour can arise near the point where homoclinic branch A disappears at a T-point. Such waves are also expected in the De Young Keizer model. Sneyd et al. conclude that homoclinic branch

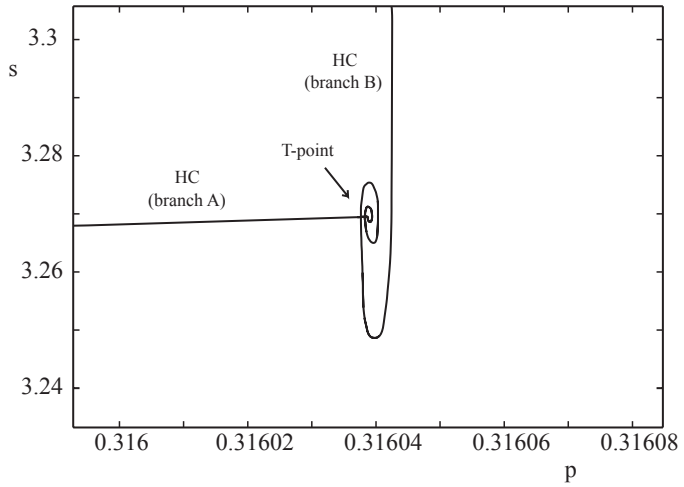

Fig. 5. Magnified view of the upper part of figure 3 where homoclinic branch A connects to homoclinic branch B at a T-point.

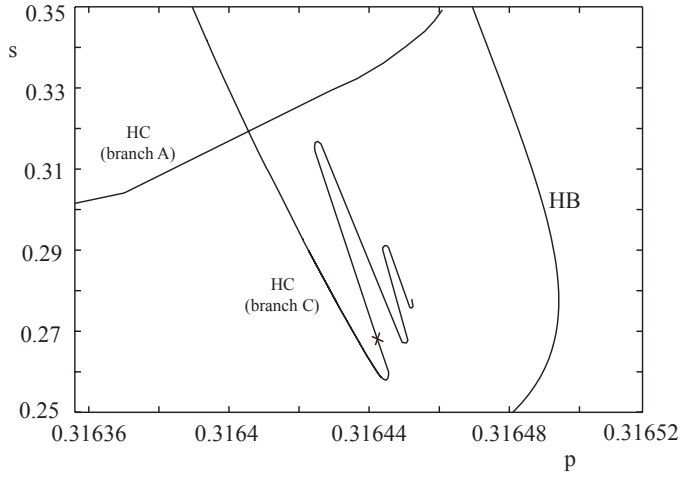

Fig. 6. Magnified view of the lower part of homoclinic branch C, showing the folding of the branch as it approaches a locus of Hopf bifurcation points..

A is the one that generates physiologically significant travelling waves. Our stability analysis would also suggest that one may restrict attention to the faster branch.

By treating the period of oscillations as a parameter it is also possible to construct dispersion curves showing the speed of a wave as a function of its period. In figure 8 we present a typical dispersion curve, $s = s(\Delta)$, for a periodic orbit. A numerical calculation of the eigenspectrum of $\mathcal{M}$

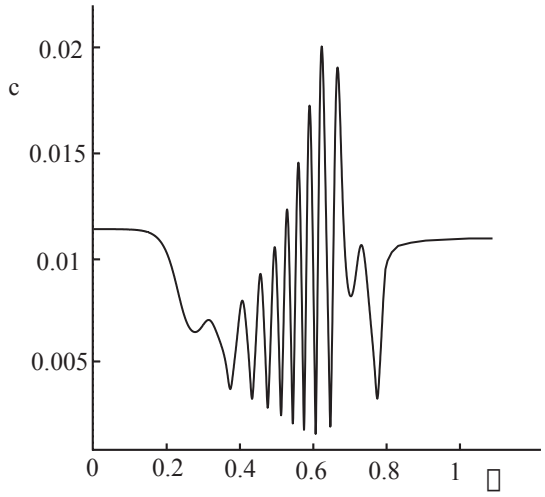

Fig. 7. A Homoclinic orbit from the marked point in figure 6.

shows that it is the faster of the two branches that is stable. Knowledge of

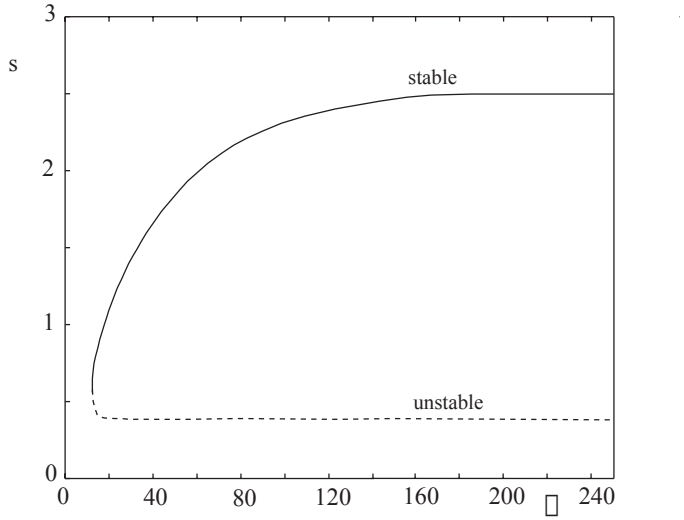

Fig. 8. The dispersion curve for periodic travelling waves when $p = 0.2622$.

dispersion curves opens the way for the development of a *kinematic* theory of irregular wave propagation that attempts to follow irregularly spaced spikes

of activity (Rinzel and Maginu [1984]). In this approach the dynamics of Ca^{2+} *spikes* are considered to evolve according to

$$\frac{\mathrm{d}T^n}{\mathrm{d}x} = \frac{1}{s(\Delta^n)}, \qquad \Delta^n(x) = T^n(x) - T^{n-1}(x), \tag{13}$$

where the time at which the nth spike occurs at position x is defined in terms of a threshold parameter $c_{\rm th}$ as

$$T^n(x) = \inf\{\ t \mid c(x,t) \geq c_{\rm th},\ \frac{\partial c(x,t)}{\partial t} > 0;\ t \geq T^{n-1}(x)\}. \tag{14}$$

We shall call $\Delta^n(x)$ the interspike interval (ISI), as it measure the time between spikes of activity at position x. A linear stability analysis of the kinematic equations shows that solutions are stable if $s'(\Delta^n) > 0$ for all n. For a periodic orbit with $\Delta^n = \Delta$ the stability predictions of the kinematic theory (solutions are stable if $s'(\Delta) > 0$, i.e. on the upper branch) are in complete agreement with those obtained from the eigenspectrum of $\mathcal{M}$. Interestingly it has been shown that when the stable branch of the dispersion curve has an exponential shape then there are solutions to the kinematic equations that describe stable connections to periodic orbits (Coombes [2001b]). This form of wave may also be regarded as a travelling front in the ISIs such that $\Delta^n(x) = \Delta(\kappa x - \omega n)$ for some κ and ω where $\Delta(z)$ has a sigmoidal shape. To confirm this prediction we perform a direct numerical simulation

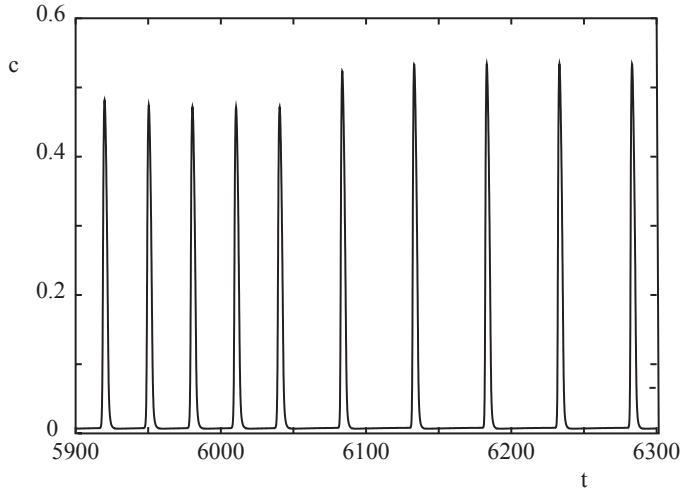

Fig. 9. Stimulation of a cell of length $L = 200$ and $p = 0.26$ with a spike train input at $x = 0$ with ISI changing from $\Delta_{(1)} = 30$ to $\Delta_{(2)} = 50$ after 200 spikes. Dynamics of Ca^{2+} is shown at a position of $3L/4$ from the point of stimulation, showing a connection between periodic orbits with ISI $\Delta_{(1)}$ and $\Delta_{(2)}$.

of the De Young Keizer model. Since we are looking for a travelling front

in the ISIs we choose initial data (at one end of a cell of length L) with a spike train that has a step change in the interspike intervals (changing from $\Delta_{(1)}$ to $\Delta_{(2)}$). An example of such a direct simulation is shown in figure 9 . Another way to visualise these connection between periodic orbits is to plot the ISIs at various values of x as a function of the number of spiking events at those position, as shown in figure 10 (where we have used values of $\Delta_{(1)}$ to $\Delta_{(2)}$ that best illustrate the sigmoidal nature of the front). Here, it is clearly seen that the step change can smooth out to form a transition layer of the form predicted by the kinematic theory.

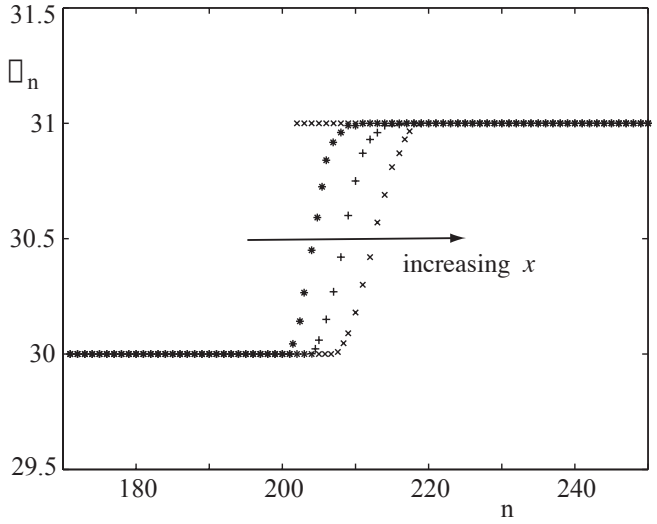

Fig. 10. Travelling front in the ISIs, showing a connection between periodic orbits. Initial data is in the form of a spike train with a step in the ISIs after 200 spikes from $\Delta_{(1)} = 30$ to $\Delta_{(2)} = 31$. Here, $p = 0.26$ and $c_{\rm th} = 0.3$. Data is represented at the following positions: 0, $L/4$, $L/2$ and $3L/4$, with $L = 200$.

In the next section we introduce a minimal FDF type model of Ca^{2+} release that exhibits many of the waves we have just described for the De Young Keizer model. Analytically obtained wave solutions corresponding to pulses, periodics and connections to periodics are shown to behave qualitatively like those in the De Young Keizer model under parameter variation. Moreover, the simplicity of the model means that it is also possible to perform a full linear stability analysis of all travelling wave solutions.

4. A fire-diffuse-fire type model

The FDF model of Keizer et al. (1998) was originally introduced as a minimal model of spark-mediated Ca^{2+} waves. In one dimension the model may

be written in the form

$$\frac{\partial u}{\partial t} = -\frac{u}{\tau_d} + D\frac{\partial^2 u}{\partial x^2} + \rho(x)\sum_m \eta(t - T^m(x)), \tag{15}$$

where $u = [\mathrm{Ca}^{2+}]$. The function $\rho(x)$ describes the distribution of Ca^{2+} release sites, and τ_d^{-1} is the rate at which Ca^{2+} is pumped back into the stores. Note that in comparison to the De Young Keizer model, the model of a pump is linear and is one of the reasons why the model is mathematically tractable. The other reason is that there is no explicit inclusion of a receptor dynamics. Rather, Ca^{2+} puffs are triggered from the release site at position x at times $T^m(x)$, $m \in \mathbb{Z}$. These release times are defined in terms of a threshold process according to

$$T^m(x) = \inf\{\ t \mid u(x,t) > h,\ \frac{\partial u(x,t)}{\partial t} > 0;\ t \geq T^{m-1}(x)\}. \tag{16}$$

The function $\eta(t)$ describes the shape of the puff and is often considered to be a simple rectangle:

$$\eta(t) = \frac{\sigma}{\tau_R}\Theta(t)\Theta(\tau_R - t), \tag{17}$$

where σ is the strength of the puff and τ_R its duration. Because of its threshold nature, waves in the FDF model may be generated by a form of CICR. In contrast, biological mechanisms of CICR typically arise when a receptor channel is activated at a low cytosolic Ca^{2+} level and inhibited at a higher one. For low Ca^{2+} levels, an increase in Ca^{2+} stimulates a further increase. At higher levels receptors inactivate and cannot reopen for some time during which they are said to be in a *refractory* state. Thus, the release of Ca^{2+} by intracellular stores is self-regulating. As it stands the FDF model ignores this physiologically important process and cannot therefore be sensibly used to understand periodic travelling waves. It is of course perfectly satisfactory when studying solitary waves, since single release events are not affected by refractoriness. To remedy this lack of refractoriness we introduce a time dependent threshold. The idea is to mimic refractoriness, whilst retaining analytical tractability, with a threshold which is high just after a release event but gradually decays back to some more normal level. Such a process may be written

$$\dot{h} = \frac{u_{\mathrm{th}} - h}{\tau} + \gamma\sum_m \delta(t - T^m(x)), \tag{18}$$

where τ determines the refractory time-scale and γ is some large positive constant. Using this scheme h decays towards a constant threshold u_{th} at a rate τ^{-1} and $h \to \gamma h$, whenever a Ca^{2+} puff is triggered.

A further weakness of the FDF model is that it is independent of IP_3 concentration, which as we have seen is an important parameter of the De Young Keizer model. To include a notion of IP_3 sensitivity within an FDF

model it is natural to modify the threshold parameter, such that release events are easier to generate in the presence of high IP_3. We suggest that the level of Ca^{2+} in the endoplasmic reticulum, c_{er}, required to generate a periodic travelling wave is a good candidate for determining a threshold function $u_{th} = u_{th}(p)$. In figure 11 we continue Hopf and limit points of figure 3 that define the borders of such a region in the (p, c_{er}) parameter plane. This figure shows that for small values of IP_3 waves fail to propagate and that lower levels of c_{er} are required to generate waves with increasing $[IP_3]$, as observed experimentally. We approximate the threshold function

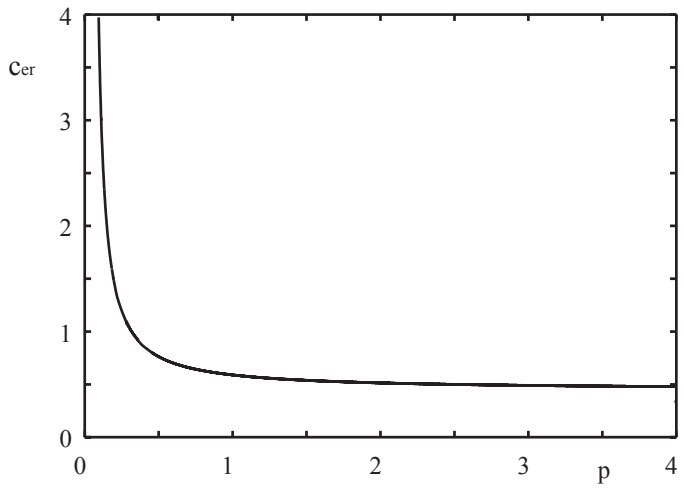

Fig. 11. Concentration of calcium in the endoplasmic reticulum, c_{er}, as a function of IP_3 concentration, p, in the De Young Keizer model, required to generate travelling waves.

of figure 11 using

$$u_{th}(p) = u_0 + A\frac{e^{-Bp}}{p - C}, \tag{19}$$

where $u_0 = 0.48$, $A = 0.1627$, $B = 0.5583$ and $C = 0.055$ are fitted numerically. The inclusion of an IP_3 dependent threshold level in the FDF model makes it sensitive to IP_3 and allows a more direct comparison with results from the De Young Keizer model.

4.1. Continuum model

Let us first construct periodic waves in our generalised FDF model when $\rho(x) = 1$, i.e. a simple continuum model. In the language of release events these waves are described by solutions of the form $T^m(x) = (m + kx)\Delta$,

where k is the wavenumber and $s = 1/(k\Delta)$ the wave velocity. Assuming $u(x,t) = u(\xi)$, where $\xi = st - x$, gives the following travelling wave ODE:

$$Du_{\xi\xi} - su_\xi - \frac{u}{\tau_d} = -\frac{\sigma}{\tau_R}\Theta(\xi)\Theta(s\tau_R - \xi), \tag{20}$$

where $u_\xi \equiv \mathrm{d}u/\mathrm{d}\xi$. The solution to (20) takes the form $u(\xi) = u(\xi + m\Delta)$:

$$u(\xi) = \begin{cases} \alpha_1 \mathrm{e}^{\lambda_+\xi} + \alpha_2 \mathrm{e}^{\lambda_-\xi} + \tau_d\sigma/\tau_R & 0 < \xi < s\tau_R \\ \alpha_3 \mathrm{e}^{\lambda_+\xi} + \alpha_4 \mathrm{e}^{\lambda_-\xi} & s\tau_R < \xi < s\Delta, \end{cases} \tag{21}$$

with

$$\lambda_\pm = \frac{1}{2D}\left[s \pm \sqrt{s^2 + 4D/\tau_d}\right]. \tag{22}$$

By demanding continuity of the solution and its first derivative the coefficients $\alpha_1 \ldots \alpha_4$ may be found as follows

$$\alpha_1 = \frac{\tau_d\sigma}{\tau_R}\frac{\lambda_-}{(\lambda_- - \lambda_+)}\frac{(1 - \mathrm{e}^{\lambda_+ s(\Delta - \tau_R)})}{(\mathrm{e}^{\lambda_+ s\Delta} - 1)} \tag{23}$$

$$\alpha_2 = -\frac{\tau_d\sigma}{\tau_R}\frac{\lambda_+}{(\lambda_- - \lambda_+)}\frac{(1 - \mathrm{e}^{\lambda_- s(\Delta - \tau_R)})}{(\mathrm{e}^{\lambda_- s\Delta} - 1)} \tag{24}$$

$$\alpha_3 = \frac{\tau_d\sigma}{\tau_R}\frac{\lambda_-}{(\lambda_- - \lambda_+)}\frac{(1 - \mathrm{e}^{-\lambda_+ s\tau_R})}{(\mathrm{e}^{\lambda_+ s\Delta} - 1)} \tag{25}$$

$$\alpha_4 = -\frac{\tau_d\sigma}{\tau_R}\frac{\lambda_+}{(\lambda_- - \lambda_+)}\frac{(1 - \mathrm{e}^{-\lambda_- s\tau_R})}{(\mathrm{e}^{\lambda_- s\Delta} - 1)}. \tag{26}$$

The self-consistent speed of the periodic travelling wave may be found by demanding $u(s\Delta) = h$. This generates an implicit equation for the dispersion relation $s = s(\Delta)$:

$$\widetilde{u}\frac{1 - \mathrm{e}^{-\Delta/\tau}}{1 - \gamma\mathrm{e}^{-\Delta/\tau}} = \frac{\lambda_-}{(\lambda_- - \lambda_+)}\frac{(1 - \mathrm{e}^{-\lambda_+ s\tau_R})}{(\mathrm{e}^{\lambda_+ s\Delta} - 1)} - \frac{\lambda_+}{(\lambda_- - \lambda_+)}\frac{(1 - \mathrm{e}^{-\lambda_- s\tau_R})}{(\mathrm{e}^{\lambda_- s\Delta} - 1)}, \tag{27}$$

where $\widetilde{u} = u_{\mathrm{th}}(p)\tau_R/\tau_d\sigma$. We plot a typical dispersion curve in figure 12, showing a similar shape to that of the De Young Keizer model (see figure 8). No attempt has been made to tune free parameters of the FDF model to obtain a quantitative fit. We invoke the model independent kinematic theory presented earlier to establish that it is the faster of the two possible branches that is stable. Moreover, since the stable branch of the dispersion curve has an exponential shape stable waves representing connections to periodics are also expected. Note that if we neglect refractoriness and consider a constant threshold the resulting dispersion curve exhibits unphysical divergent speeds. This is expected in the absence of a refractory process since release events can occur arbitrarily close in time.

In a similar fashion we may construct solitary pulses defined by $T^1(x) = x/s$ or just take the limit $\Delta \to \infty$ of periodic travelling waves. In figure 13 we plot the wave speed of a pulse as a function of the IP_3 concentration. For

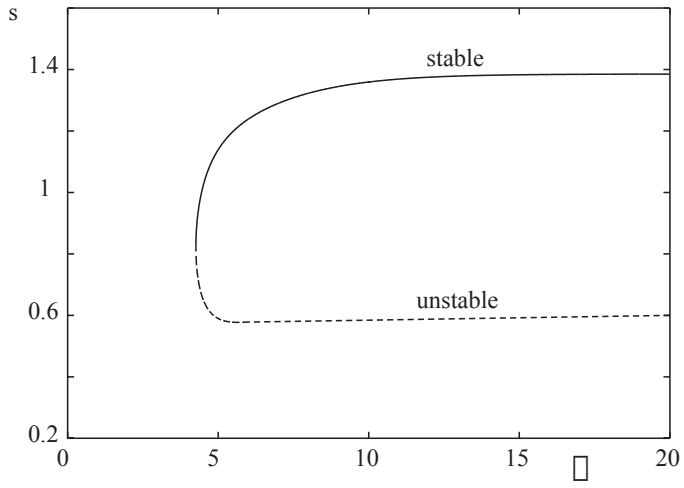

Fig. 12. The dispersion curve obtained from (27) when $\widetilde{u} = 0.2$, $\tau = 2$, $\gamma = 3$, $\tau_R = 1$, $\tau_d = 1$ and $D = 1$.

a comparison between the De Young Keizer model and the generalised FDF model we choose the same diffusion coefficient and adjust the remaining time and strength scales appropriately. A value for τ_R is chosen simply by reading off the temporal duration of a calcium spike in the De Young Keizer model. The time scale of the linear pump in the FDF model is chosen so as best to agree with that of nonlinear pump term in equation (1). This term is sigmoidal with a slowly varying gradient for intermediate levels of calcium concentration. The gradient in this intermediate regime provides a reasonable estimate for τ_d. This leaves only one free parameter, namely $\widetilde{u}$, which we choose so as to give the best quantitative agreement of the generalised FDF and De Young Keizer models (compare figures 3 and 13). In the absence of an IP_3 dependent threshold function no such comparison would have been possible. Hence, the generalised FDF model (with parameters given in the caption of figure 13) that we have presented can capture many of the wave solutions present in the more complicated De Young Keizer model. The analytical tractability of the model also opens up the possibility to study more realistic distributions of release sites.

4.2. Discrete model

One of the major advantages of the FDF model is to account for both saltatory and continuous travelling waves. Unlike continuous waves, saltatory ones do not travel with a constant profile. They arise when the translation symmetry of the model is broken, say with the inclusion of stores at discrete points in space. For simplicity we consider an idealised set of point sources so that $\rho(x) = \sum_n \delta(x - nd)$, where d is the spacing between stores. The

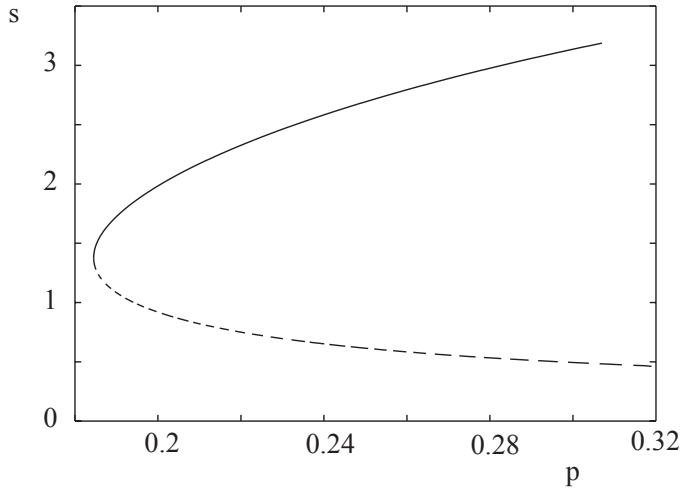

Fig. 13. Speed of the travelling pulse in the FDF continuum model as a function of $[IP_3]$ with $\widetilde{u} = 0.17 u_{\rm th}(p)$, $\tau_R = 0.5$, $\tau_d = 0.29$ and $D = 1$.

solution to the FDF model can be expressed using Green's functions as

$$u(x,t) = \frac{\sigma}{\tau_R} \sum_{n=-\infty}^{\infty} \sum_{m=0}^{\infty} \int_{T^m(x_n)}^{T^m(x_n)+\tau_R} G(x-nd, t-t') {\rm d}t', \qquad (28)$$

where

$$G(x,t) = \frac{{\rm e}^{-t/\tau_d}}{\sqrt{4\pi D t}} {\rm e}^{-x^2/(4Dt)} \Theta(t). \qquad (29)$$

We consider periodic travelling waves that satisfy $T^m(nd) = nd/s + m\Delta = n\Delta_1 + m\Delta$, where s is the speed of threshold crossing events given by $s = d/\Delta_1$ and Δ is the time between successive Ca^{2+} release events at a store. For simplicity we shall consider Δ to be sufficiently large that we do not have to worry about the inclusion of refractory processes and take the threshold for release to be $u_{\rm th}(p)$. The solution describing saltatory periodic travelling waves in the FDF model is

$$u(x,t) = \frac{\sigma}{\tau_R} \sum_{n,m} \int_0^{\min(t-n\Delta_1-m\Delta,\tau_R)} G(x-nd, t-t'-n\Delta_1-m\Delta) {\rm d}t'. \quad (30)$$

Generalising the analysis of a saltatory travelling pulse presented in (Coombes [2001a]) shows that the speed of the wave is implicitly determined by

$$u_{\rm th}(p) = \sigma \sum_{n=0}^{\infty} \sum_{m=0}^{\infty} H(nd, n\Delta_1 + m\Delta), \qquad (31)$$

where

$$H(x,t) = \frac{1}{\tau_R} \int_0^{\tau_R} G(x, t-t') {\rm d}t'. \qquad (32)$$

In the special case $\tau_R \to 0$ we see from (32) that $H(x,t) \to G(x,t)$. For finite τ_R, the function $H(x,t)$ is evaluated in (Coombes [2001a]) as $H(x,t) = A(x,t-\tau_R) - A(x,t)$, where

$$A(x,t) = \frac{\sqrt{\tau_d D}}{4D\tau_R}\left[\exp\left(\frac{-|x|}{\sqrt{\tau_d D}}\right)\mathrm{erfc}\left(-\frac{|x|}{\sqrt{4Dt}}+\sqrt{\frac{t}{\tau_d}}\right)\right.$$
$$\left.+\exp\left(\frac{|x|}{\sqrt{\tau_d D}}\right)\mathrm{erfc}\left(\frac{|x|}{\sqrt{4Dt}}+\sqrt{\frac{t}{\tau_d}}\right)\right]. \qquad (33)$$

A saltatory periodic travelling wave determined by (30) and (31) is shown in figure 14. This nicely illustrates that waves propagate with a non-constant profile and that large increase in Ca^{2+} concentration occur just after a release event.

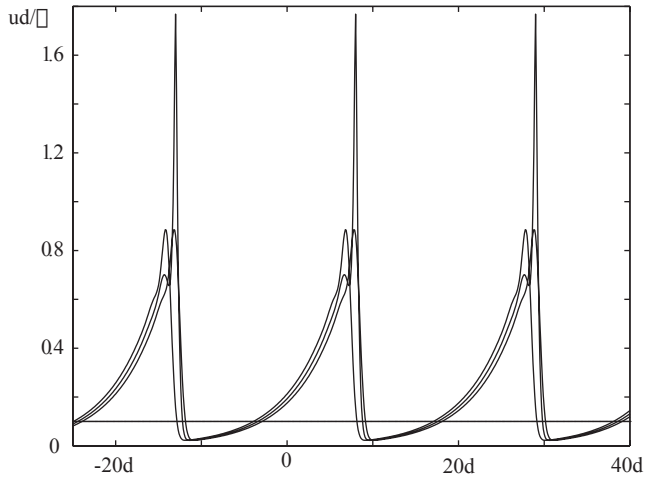

Fig. 14. An example of a stable saltatory periodic travelling wave. The period Δ_1 is determined self-consistently as $\Delta_1 = 0.2$. Other parameters are $\tau_d = 1$, $d^2/D = 1$, $\tau_R = 0.1$, $\Delta = 4.2$ and $u_{\rm th}(p)d/\sigma = 0.1$. The system is sampled at some large release time t_0, then at $t_0 + \tau_R$ and $t_0 + \Delta_1$.

In figure 15 we show how the period of travelling waves depends on the value of τ_d^{-1} for the case that $\tau_R = 0$. We see that there is propagation failure at some critical value of τ_d, where two branches of the solutions coalesce. To illustrate the effects of a finite width for the calcium puff on the speed of the periodic travelling wave we continue the limit point of the bifurcation diagram in figure 15 as a function of τ_R. The results of numerical continuations are shown in figure 16. This plot shows the parameter region where saltatory periodic travelling waves can exist and highlights the fact that with increasing τ_R the limit point in 15 occurs at increasingly larger values of τ_d.

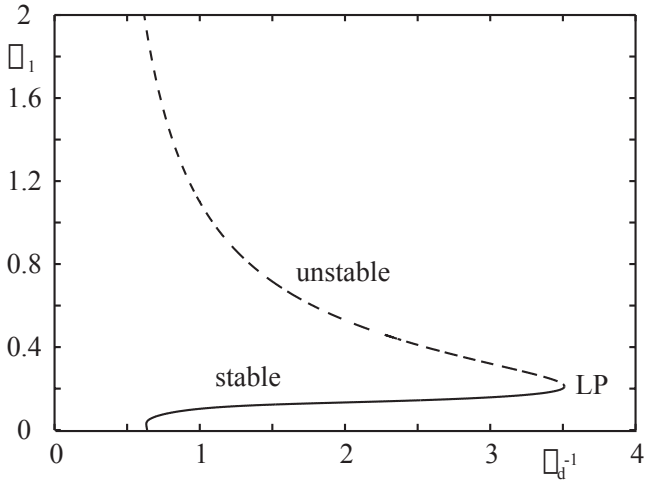

Fig. 15. Period Δ_1 as a function of the parameter τ_d^{-1} with $\tau_R = 0$. Other parameters as in figure 14.

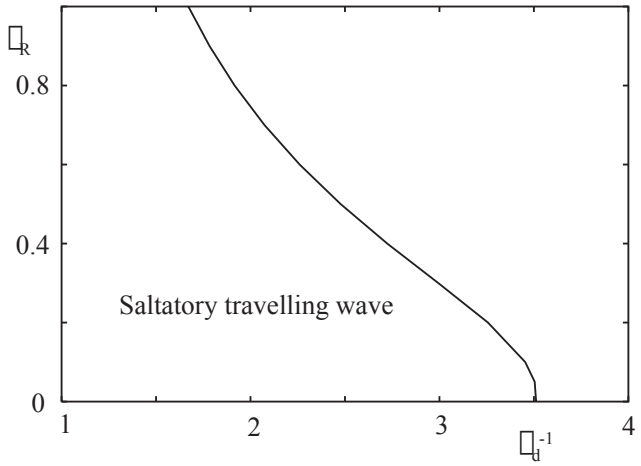

Fig. 16. Continuation of the limit point of figure 15 in the (τ_d^{-1}, τ_R) plane.

The fact that there are two solution branches for a periodic travelling wave raises the question of stability. To determine the stability of saltatory waves we consider perturbation of the release times where $T^m(nd) \to T^m(nd) + \delta_n e^{m\lambda}$, $\lambda \in \mathbb{C}$, and examine the linearised evolution of these perturbations. We restrict our attention to the class of perturbations where $\delta_n = 1$ for all n. Solutions are linearly stable if $\mathrm{Re}\,\lambda < 0$. After substituting

into (31) and expanding to first order we obtain

$$\Phi(\alpha,\beta) \equiv \sum_{n,m} \mathrm{e}^{m\alpha}\mathrm{e}^{im\beta} H'(nd, n\Delta_1 + m\Delta) = 0. \tag{34}$$

where we have set $\lambda = \alpha + \mathrm{i}\beta$, $\alpha, \beta \in \mathbb{R}$. Here, $H'(x,t) = \partial H(x,t)/\partial t$. Differentiation of (32) shows that $H'(x,t) = [G(x,t) - G(x,t-\tau_R)]/\tau_R$. To find the stability of the solution as a function of system parameters the system of two equations $\mathrm{Re}\,\Phi(\alpha,\beta) = 0$ and $\mathrm{Im}\ \Phi(\alpha,\beta) = 0$ has to be solved simultaneously for α and β along the solution branch. Two possible types of bifurcation point are defined by the conditions $\alpha = 0, \beta = 0$ and $\alpha = 0, \beta \neq 0$. For the first case a change in stability occurs when $\Phi(0,0) = 0$. The second type of instability arises when a complex eigenvalue crosses the imaginary axis. Then a change of stability occurs when $\beta = \pi$. A plot of the function $\Phi(0,\pi)$ in figure 17 shows that the change of stability for the solution shown in figure 15 occurs at the limit point defining propagation failure. A direct examination of $\alpha = \mathrm{Re}\,\lambda$, along the two solution branches,

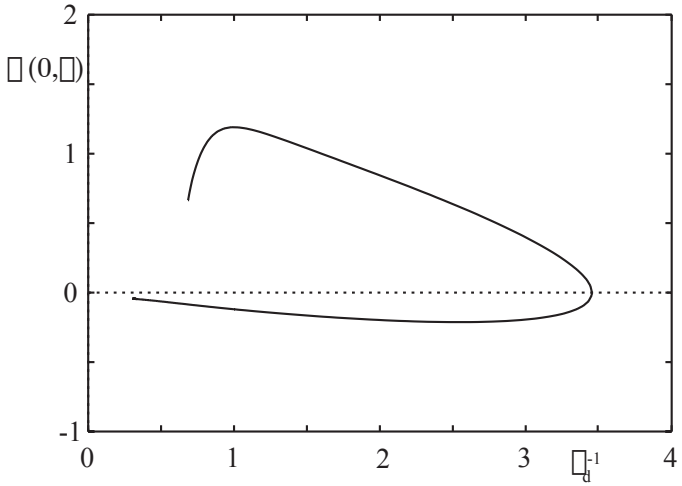

Fig. 17. A plot of the function $\Phi(0,\pi)$ along the solution of figure 15, showing that there is a change in stability at the limit point where propagation failure occurs.

shows that the faster branch is stable, while the slower one is unstable.

5. Discussion

In this paper we have presented a detailed numerical bifurcation analysis of travelling waves in the reduced De Young Keizer model of calcium release. The linear stability of these waves has been found by numerically solving

an appropriate eigenvalue problem. A by-product of this investigation is the observation that this model has qualitatively the same dynamics as the recently introduced two-state model of IP_3 receptor dynamics (Sneyd et al. [2000]) for pancreatic acinar cells. We have also shown, using a kinematic theory, that models of this type will support travelling waves that connect periodic orbits. We have used a detailed numerical analysis to motivate the form of a minimal FDF model capable of exhibiting qualitatively similar behaviour. An important feature of this FDF model is the inclusion of a dynamic IP_3 sensitive threshold. The main advantage of studying FDF models is their mathematical tractability. Indeed the explicit construction of stable travelling periodic waves has allowed us to probe the mechanisms for propagation failure in the two extremes of i) a continuous distribution of calcium stores and ii) a discrete distribution. Now that we have established the usefulness of using generalised FDF models for studying propagation of Ca^{2+} it opens up new possibilities for mathematical progress in the field of intracellular signalling. In particular the FDF model may be naturally extended to include further layers of biological reality. These important extensions include more general choices of the distribution of release sites, the stochastic triggering of release and studying the model in two and three dimensions.

The effect of discrete, asymmetric distributions of calcium stores and anisotropic Ca^{2+} diffusion has been numerically investigated by Bugrim et al. (1997). They demonstrate that disordered distributions can lead to irregular propagation of waves. The inclusion of disorder within an FDF model is achieved in a straightforward manner by an appropriate choice of the function $\rho(x)$. One may then use scaling techniques along the lines developed in (Pencea and Hentschel [2000]) for CICR models (without IP_3 sensitivity) to produce criterion for wave propagation as a function of disorder. The stochastic triggering of release has been investigated in relatively few papers. Notable exceptions are the papers by Keizer and Smith (1998) and Falcke et al. (2000), who numerically combine stochastic simulations of Ca^{2+} release with deterministic current balance equations. More recently a model of stochastic release has been introduced using the notion that the probability of release depends algebraically on the local Ca^{2+} concentration (Izu et al. [2001]). This second approach can be incorporated within an FDF framework by treating the threshold as a random variable. Interestingly a simple stochastic model for IP_3 clusters has been shown to support waves that have statistics associated with the class of directed percolation (DP) models (Bär et al. [2000]. This then begs the question as to whether a stochastic FDF model will also generate waves belonging to the DP universality class. Finally, it is unlikely that Ca^{2+} waves are restricted to one dimensional z-lines as assumed in the FDF model discussed here. The FDF model may be easily extended to two or three dimensions and its mathematical analysis may proceed in a similar fashion to the one dimensional model. Of course, in higher dimensions the model will not only support travelling plane waves but is likely to support circular and spiral motion.

These more exotic solutions can be treated using the techniques for plane waves once an appropriate ansatz for the release times is identified. The analysis of these three further important extensions to the FDF model will be presented elsewhere.

Acknowledgements. We would like to thank Greg Smith for providing the parameters of the De Young Keizer model given in table 1.

References

N Allbritton and T Meyer. Localized calcium spikes and propagating calcium waves. *Cell Calcium*, 14:691–697, 1993.

N J Balmforth, G R Ierley, and E A Spiegel. Chaotic pulse trains. *SIAM Journal on Applied Mathematics*, 54:1291–1334, 1994.

M Bär, M Falcke, H Levine, and L S Tsimring. Discrete stochastic modeling of calcium channel dynamics. *Physical Review Letters*, 84:5664–5667, 2000.

M J Berridge. Elementary and global aspects of calcium signalling. *Journal of Physiology*, 499:291–306, 1997.

E A Bugrim, Zhabotinsky, and I R Epstein. Calcium waves in a model with a random spatially discrete distribution of Ca^{2+} release sites. *Biophysical Journal*, 73:2897–2906, 1997.

N Callamaras, J S Marchant, X P Sun, and I Parker. Activation and co-ordination of InsP(3)-mediated elementary Ca^{2+} events during global Ca^{2+} signals in Xenopus oocytes. *Journal of Physiology*, 509:81–91, 1998.

S Coombes. The effect of ion pumps on the speed of travelling waves in the fire-diffuse-fire model of Ca^{2+} release. *Bulletin of Mathematical Biology*, 63:1–20, 2001a.

S Coombes. From periodic travelling waves to travelling fronts in the spike-diffuse-spike model of dendritic waves. *Mathematical Biosciences*, 170: 155–172, 2001b.

G W De Young and J Keizer. A single pool IP_3-receptor based model for agonist stimulated Ca^{2+} oscillations. *Proceedings of the National Academy of Sciences USA*, 89:9895–9899, 1992.

M Falcke, L Tsimring, and H Levine. Stochastic spreading of intracellular Ca^{2+} release. *Physical Review E*, 62:2636–2643, 2000.

P Glendinning and C Sparrow. T-point: a codimension two heteroclinic bifurcation. *Journal of Statistical Physics*, 43:479–488, 1986.

L T Izu, W G Wier, and C W Balke. Evolution of cardiac waves from stochastic calcium sparks. *Biophysical Journal*, 80:103–120, 2001.

J Keener and J Sneyd. *Mathematical Physiology*. Springer, 1998.

J Keizer and G W De Young. Simplification of a realistic model of IP_3-induced Ca^{2+} oscillations. *Journal of Theoretical Biology*, 166:431–442, 1994.

J E Keizer, G D Smith, S Ponce Dawson, and J Pearson. Saltatory propagation of Ca^{2+} waves by Ca^{2+} sparks. *Biophysical Journal*, 75:595–600, 1998.

Y Li and J Rinzel. Equatons for $InsP_3$ receptor mediated $[Ca^{2+}]_i$ oscillations derived from a detailed kinetic model: A Hodgkin-Huxley like formalism. *Journal of Theoretical Biology*, 166:461–473, 1994.

P Lipp and M D Bootman. To quark or to spark, that is the question. *Journal of Physiology*, 502:1–1, 1997.

C S Pencea and H G E Hentschel. Excitable calcium wave propagation in the presence of localized stores. *Physical Review E*, 62:8420–8426, 2000.

J Rinzel and K Maginu. *Non-equilibrium Dynamics in Chemical Systems*, chapter Kinematic analysis of wave pattern formation in excitable media, pages 107–113. Springer-Verlag, 1984.

J Sneyd, J Keizer, and M J Sanderson. Mechanisms of calcium oscillations and waves: a quantitative analysis. *FASEB*, 9:1463–1472, 1995.

J Sneyd, A LeBeau, and D Yule. Traveling waves of calcium in pancreatic acinar cells: model construction and bifurcation analysis. *Physica D*, 145: 158–179, 2000.

Y Tang, J L Stephenson, and H G Othmer. Simplification and analysis of models of calcium dynamics based on IP_3 - sensitive calcium channel kinetics. *Biophysical Journal*, 70:246–263, 1996.

L N Trefethen. *Spectal Methods in MATLAB*. SIAM, 2000.